# CHAPTER 3

Study Program

PART A: Experimental Study

3.1 Introduction

From the previous chapter, most studies exhibit that the performance of precast connection greatly influences the overall behavior of precast structural system. From the reason, an experimental study is important part for revealing the performance in each precast connections having difference details under simulate ground motion. In the study, the seven concrete subassemblies could be classified according to construction process into two groups: cast-in-place and prefabrication system. The one monolithic specimen with seismic reinforcement detail and six precast specimens with different joint detail were carefully tested under quasi-static cyclic loading according to ACI T1.1-01. Normally, there are three types of seismic load testing i.e. shake table testing, pseudo dynamic testing and quasi-static cyclic load testing. They are widely used in experimental study of structures and structural assemblages in laboratories. Park(1989) had reported that the quasi-static loading procedure is conservative estimation of the real strength of the test structure because the dynamic loading of real earthquake ground motion increases in the strain rate, resulting in an increase in the strength of the material. To observe the displacement of the concrete elements and elongation of steel reinforcement, several measuring devices such as LVDTs, PI-gauges and strain gauges were installed in each test specimen. After the experimental process, the seismic performance of all of the precast specimens were compared to the monolithic specimen. The chapter aims to describe the test procedure as expressed below.

This study conducted a test of six interior beam-column concrete specimens, which were divided into one monolithic concrete specimen and six precast concrete connections using T-section steel inserts embedded into the core of the beam-column joint. The height of each story was 3.50 m, and the bay width was 4.50 m. The beam and column sizes

41

were determined for width/depth dimensions as 300/450 mm and 200/450 mm respectively. The strong-column/weak-beam mechanism was applied in the seismic design. As shown in Figure 3.1(a), the test specimens were planar beam -column subassemblies representing a portion of the building frame at the interior joint between column and beams. Figure 3.1 (b) demonstrates the bending moments diagram of a laterally loaded moment resisting frame. In Figure 3.1 (c), maximum bending moments occur at the connection where the shear force is also at a maximum. Test specimens were subjected to lateral cyclic loads and concentrated load *H* at the top of the upper column as shown in Figure 3.1 (d) so that the bending moment and shear forces were reversed and cycled. Thus, the distribution of the bending moment in the specimens was the same as for the moment-resisting frame under cyclic loading.


(a) (b) (c) (d)
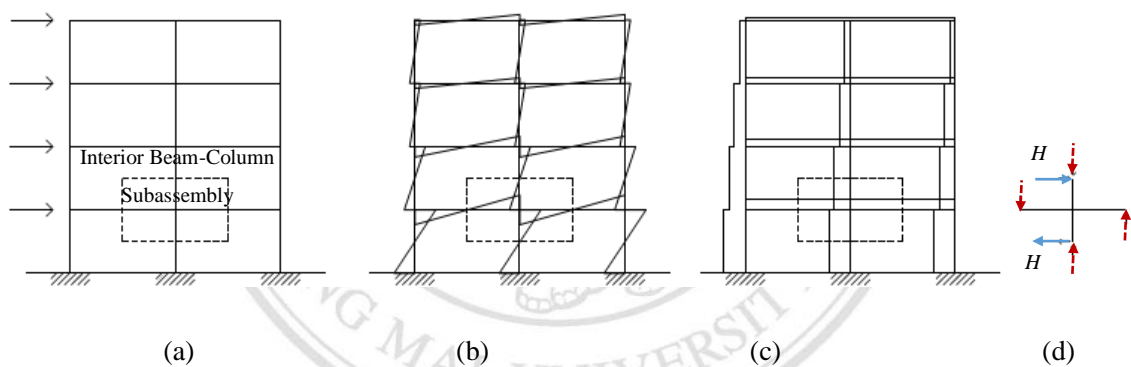
(a) Frame under lateral loads; (b) Bending moment diagram; (c) Shear force diagram;

(d) Beam-column subassembly

Figure 3.1 Frame under lateral loads

In the study, the test specimens were scaled to approximately 2/3 of the usual beam-column frame element in a prototype building. It is noted that the acceptable minimum limit scaling factor is 1/3 of the full size stated in a ACI T1.1-01 document (2001). As a result, the cross section of beam and columns in width(*b*)/depth(*h*) dimensions were 150/300 mm and 200/300 mm, respectively. The clear span of beams (shear span, *a*) was 1,350 mm and 980 mm for shear span of columns as shown in Figure 3.2. A shear span to depth ratio (*a/d*) is one of structural index, to indicate the failure mode of the element between shear and flexural failure. To enforce the failure as flexural mode, the ratio

should be high. For all test specimens, the *a/d* ratio of beams and column elements were 4.50 and 3.27, respectively. For this reason, the test specimen would fail in flexural mode.

Figure 3.2 Test specimen dimension
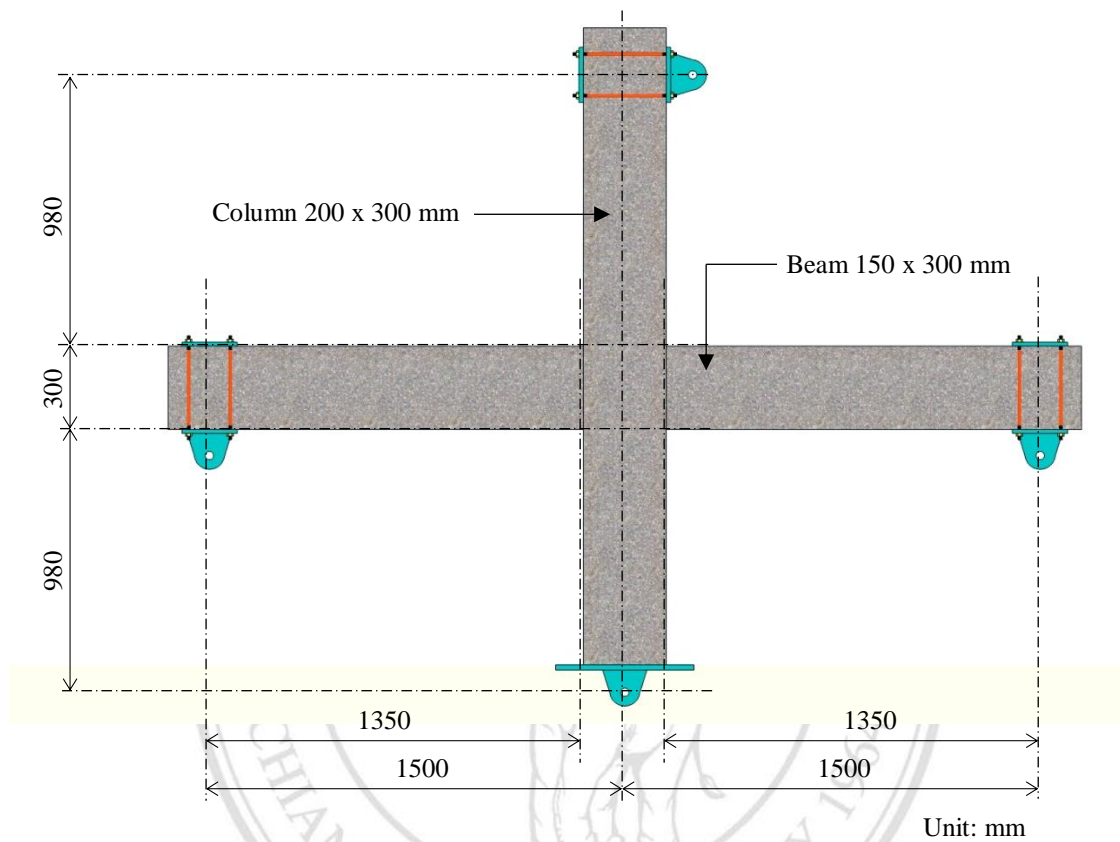
3.2 Test Setup and Test Procedure

In this study, both beam ends and the bottom of the lower column were supported by the mechanical hinges. As shown in Figure 3.3(a-b), several LVDTs were installed to measure displacements of the test specimen during the experiment and a many of PI-gauges were used to investigate shear deformations of beams, columns and joint. In addition, the strain profile of the steel reinforcement in the test specimens were observed by using strain gauges. The locations of the strain gauges are shown in Figure 3.3(c). Quasi-static cyclic testing was used to observe the structural response. The quasi-static lateral loading (*H*) was applied by a hydraulic actuator at the top of the upper column. The top column was pushed forward and pulled backward in a reversed cyclic pattern according to ACI T1.1-01. The loading history is shown in Figure 3.4. A story drift ratio, defined as ratio of the lateral displacement at the top of the column to column height, was

43

used to represent the lateral movement of the test specimens as shown in equation (3.1) and Figure3.5. The drift level was increased to 0.15%, 0.20%, 0.25%, 0.35% ... drift until the test concluded. In each story drift level, the peak amplitude was applied repeatedly for three cycles. The repeated cyclic loading was done to check the stability of the hysteresis behavior. Furthermore, a constant axial load of $0.10f'_c A_g$ or 235 kN was applied vertically at the top of the column.
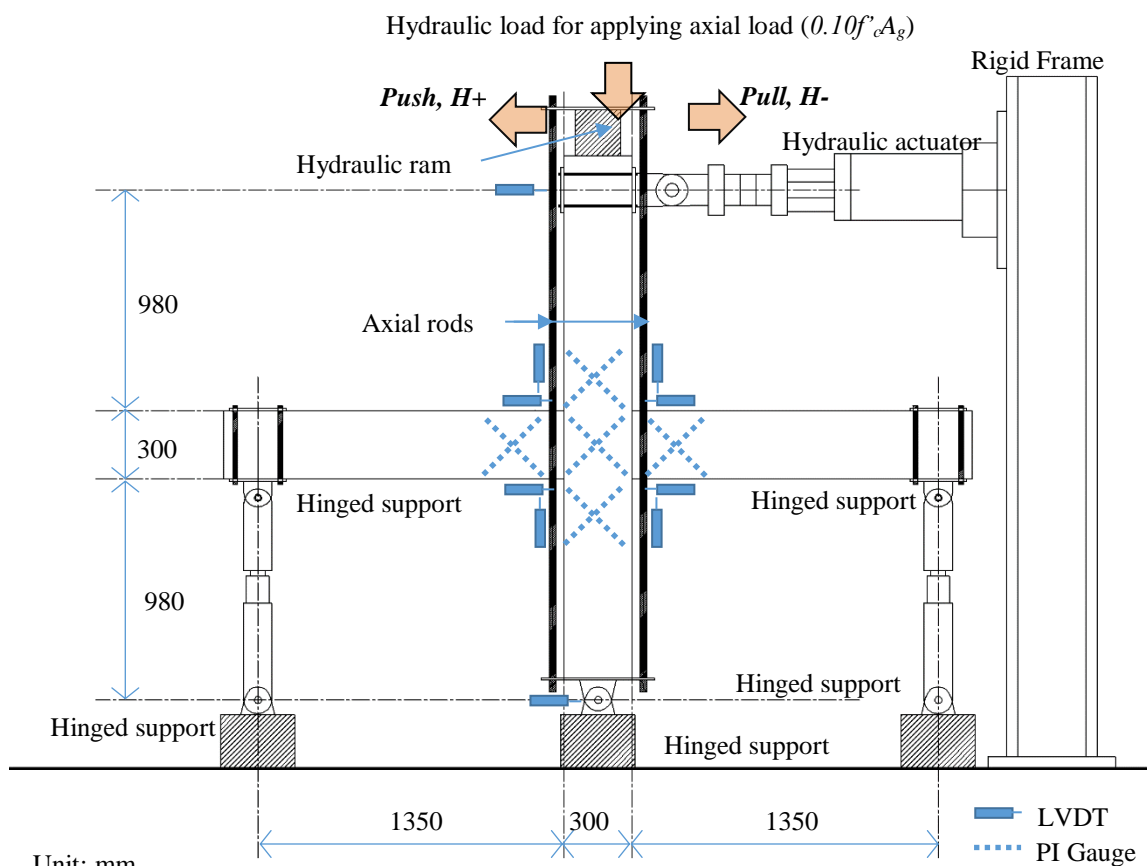
Drift ratio, $$(\theta) = \frac{(\Delta_{L1} - \Delta_{L2})}{h} \times 100 \qquad (3.1)$$

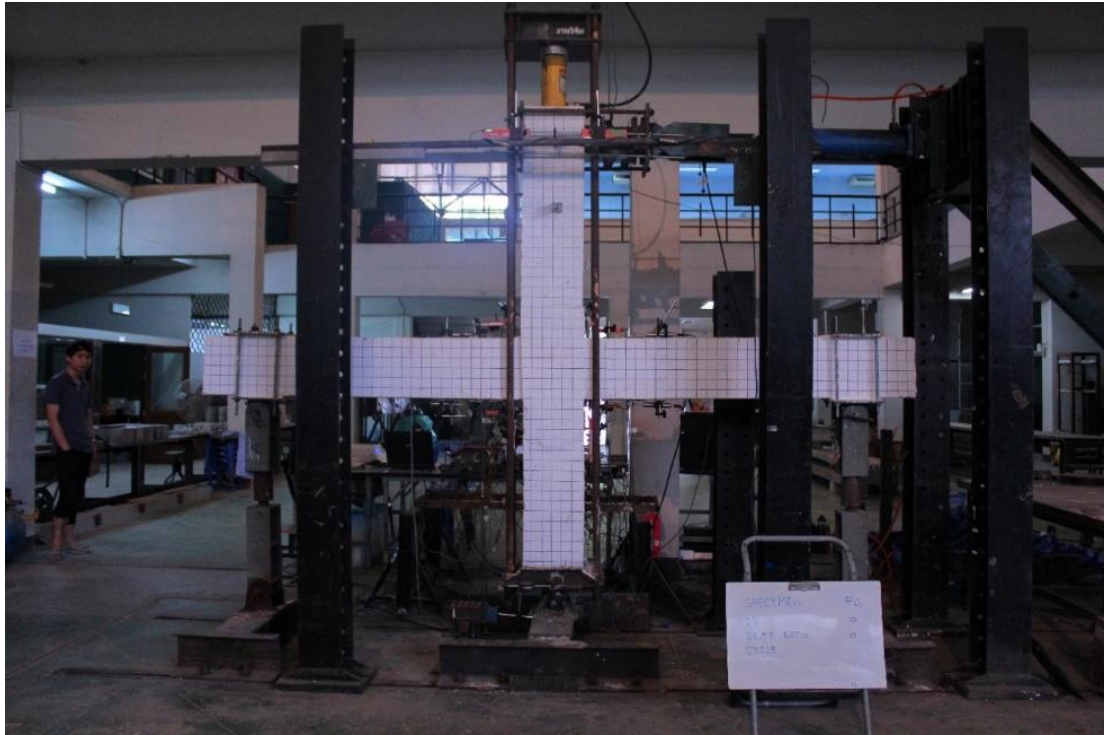where 　　(θ) = Drift ratio

　　　　Δ_{L1} = Column top displacement (mm.)

　　　　Δ_{L2} = Base displacement (mm.)

　　　　h = Column Height (mm.)

(a) 　　Configuration of test setup

(b) A view from test set up

Specimen M1

Specimen P1

Specimen P2, P3, P4

Distance a = 125 mm
Distance b = 75 mm
▲ Strain Gauge

Specimen P5 and P6
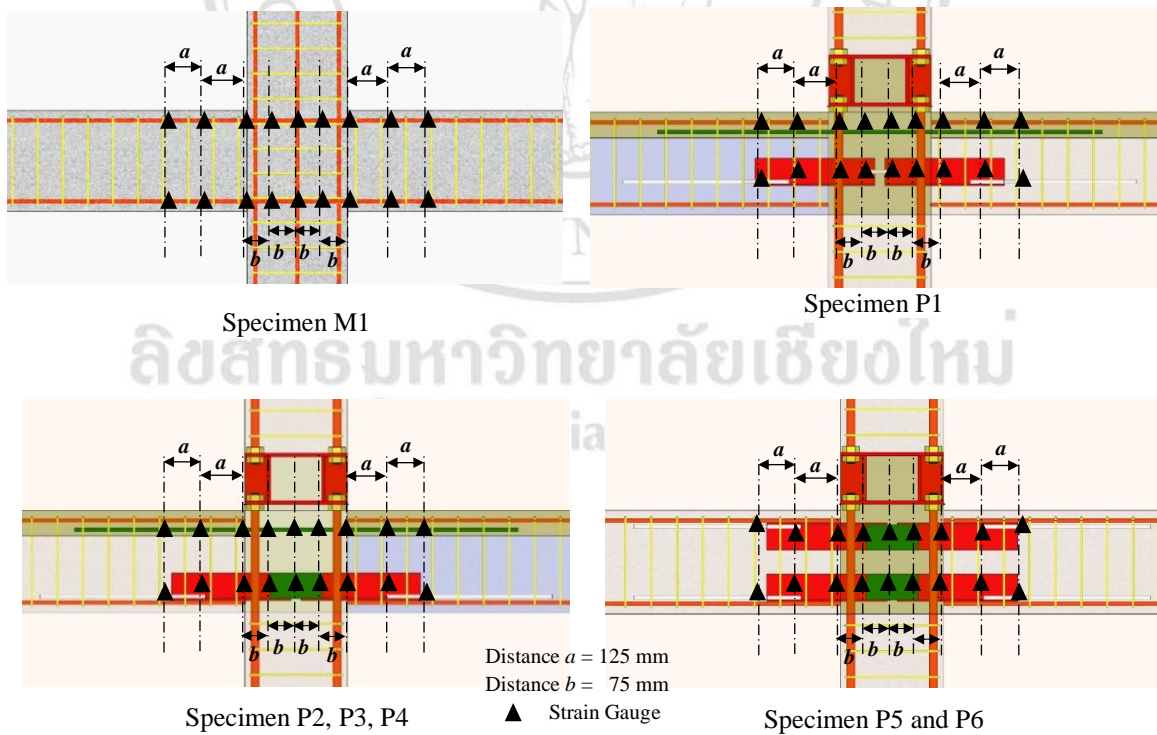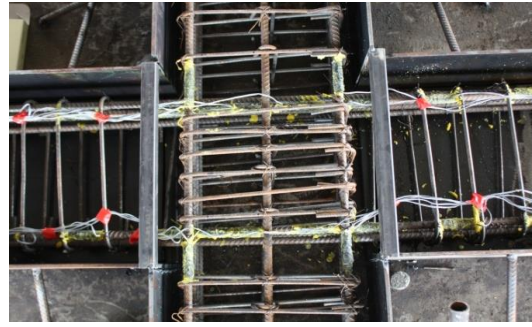
(c) Strain locations on longitudinal reinforcements

45

(d) Installing PI-gauges for measuring
deformation at joint and beams

(e) Installing strain gauges for measuring
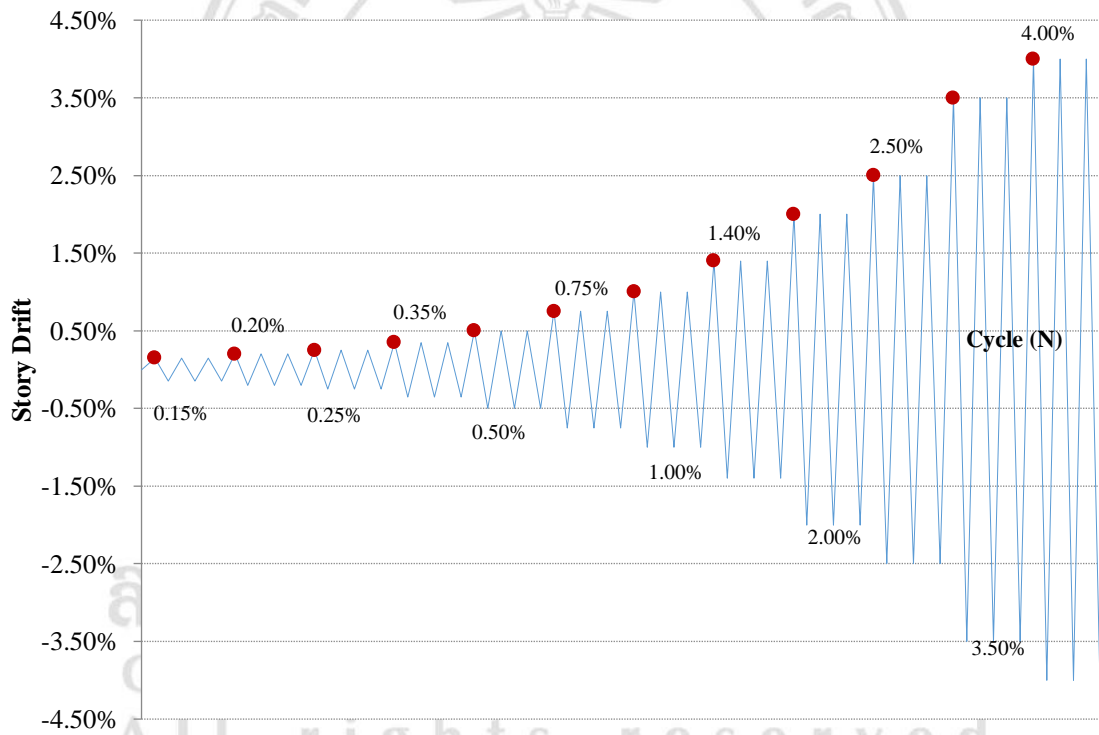elongation in rebar

Figure 3.3 Experimental setup
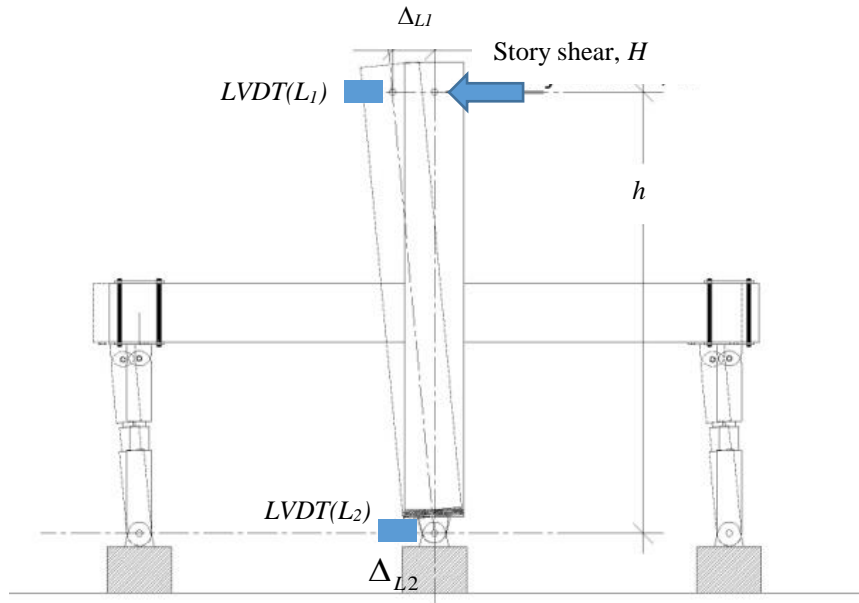

Figure 3.4 Loading history

Figure 3.5 Configuration of measuring story drift ratio

3.3 Material Properties

3.3.1 Concrete

Normal concrete was used for the production of the test specimens. Uniaxial compressive strengths were 44.03 MPa for the monolithic one and 42.97 MPa and 45.35 MPa for the beam and column precast elements, respectively. The mix proportion was as follow:

- Portland cement type 1: 393 kg/m^3
- Fly ash: 43 kg/m^3
- Water: 174 kg/m^3
- Sand: 824 kg/m^3
- Coarse aggregate (max size 19 mm): 914 kg/m^3
- Additional water reducing agent: 6.53 lite/m^3

Moreover, non-shrink grout concrete (Sikagrout 212-11, Self-leveling concrete) with a strength of 57.30 MPa was used in the precast concrete joint

47

3.3.2 Reinforcing Steel bars and steel plate

The uniaxial tension test was performed to determine their mechanical properties of reinforcing bars and steel plates forming a steel T-section insert. Table 3.1 shows a summary of the mechanical properties of the steels used in both the monolithic and precast specimens. Figure 3.6 shows a stress-strain relationship of steel reinforcement.

Table 3.1 Properties of the steel reinforcements in test specimens

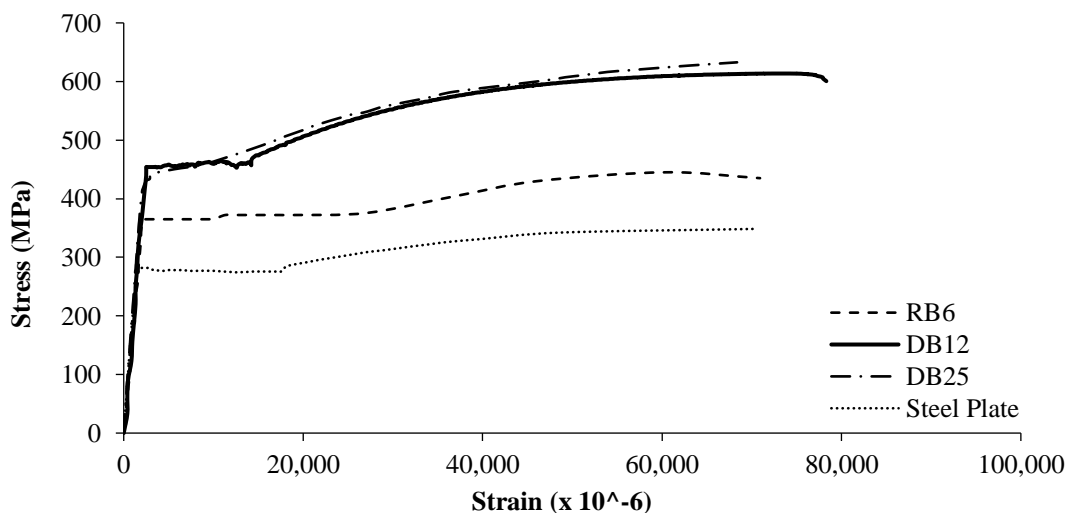|	Yield Strength (MPa)	Ultimate Strength (MPa)
RB6 (6 mm.)	364	445
DB12 (12 mm.)	455	613
DB25 (25 mm.)	442	640
Steel Plate (T-section insert)	283	348

Figure 3.6 Stress-strain relationship of steel reinforcement

3.4 Test specimen Details

In the study, test specimens were composed of one monolithic specimen and six precast concrete specimens with different connection details as shown Figure 3.7. The seismic performances of all precast specimens were compared to the monolithic control specimen. The geometries of structural elements of all specimens were designed according to the strong-column/weak-beam design philosophy. The cross section of the beam was 150 mm x 300 mm. The cross section of the column was 200 mm x 300 mm.

48

Table 3.2 describes the joint detailing, expected strength capacity and failure mode of test specimens. The expected strength capacities were calculated according to ACI 318-14 and consideration of bond-slip effect in non-shrink grout for P1 to P4 specimens. For calculating the nominal moment in the potential plastic hinge region of the precast specimens with lap splice, there were several studies about bond stress-slip response (Filippou, Popov and Bertero 1983, Esfahani and Rangan 1998, Harajli 2004, and Thai and Pimanmas 2011) suggesting that the yield strength of the lap splice was reduced to half times of steel bar. For a design experiment, the nominal strength of shear forces and flexural moments of the beams and column were compared to define the weakest element (ductile chain), failure location and mode of failure. Appendix A shows the calculation for strength capacities of all test specimens. Figures 3.8 (a-b) show the dimensions and reinforcement details of both the monolithic specimen (M1) and all of the precast specimens (P1-P6).
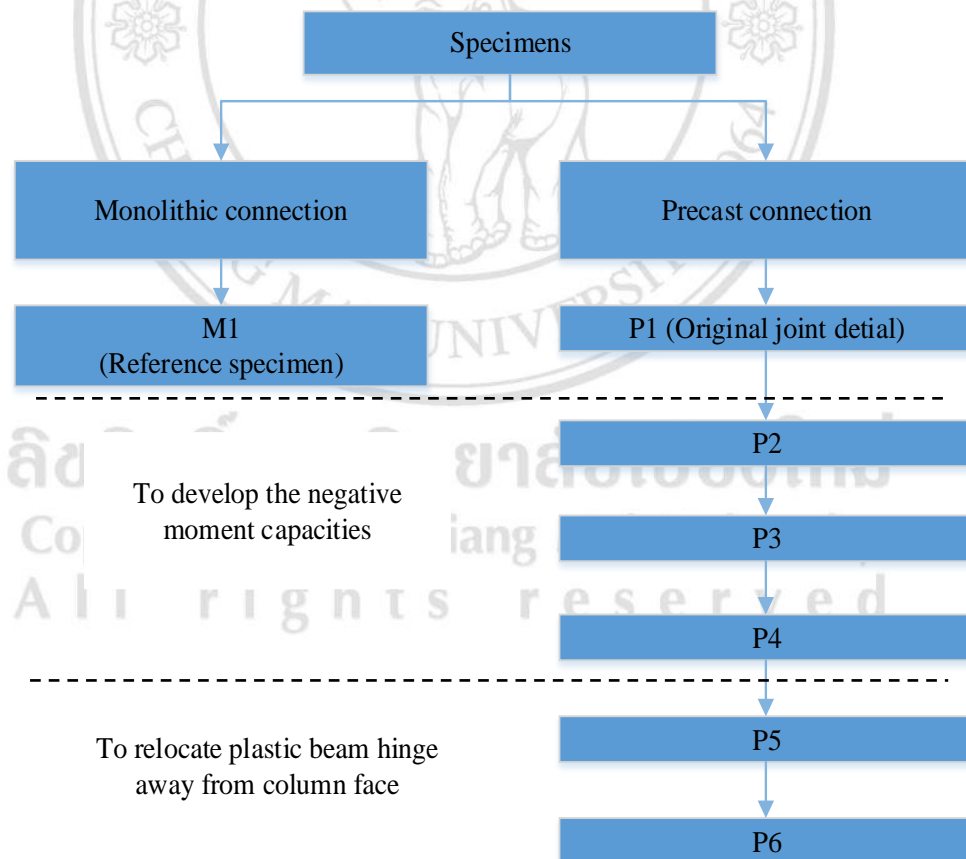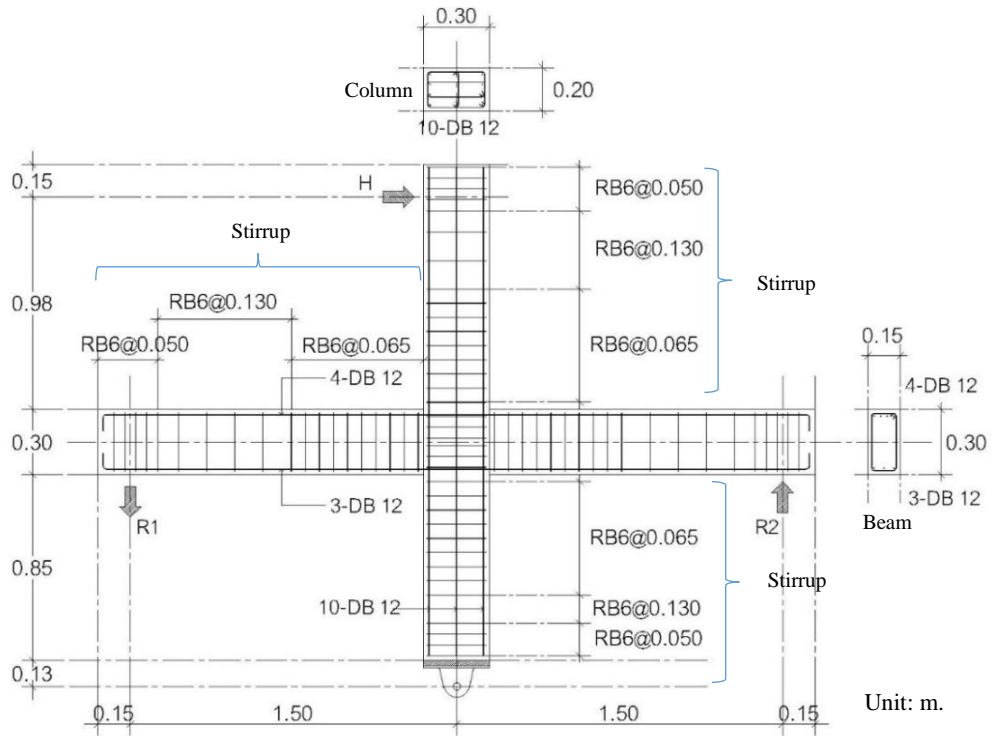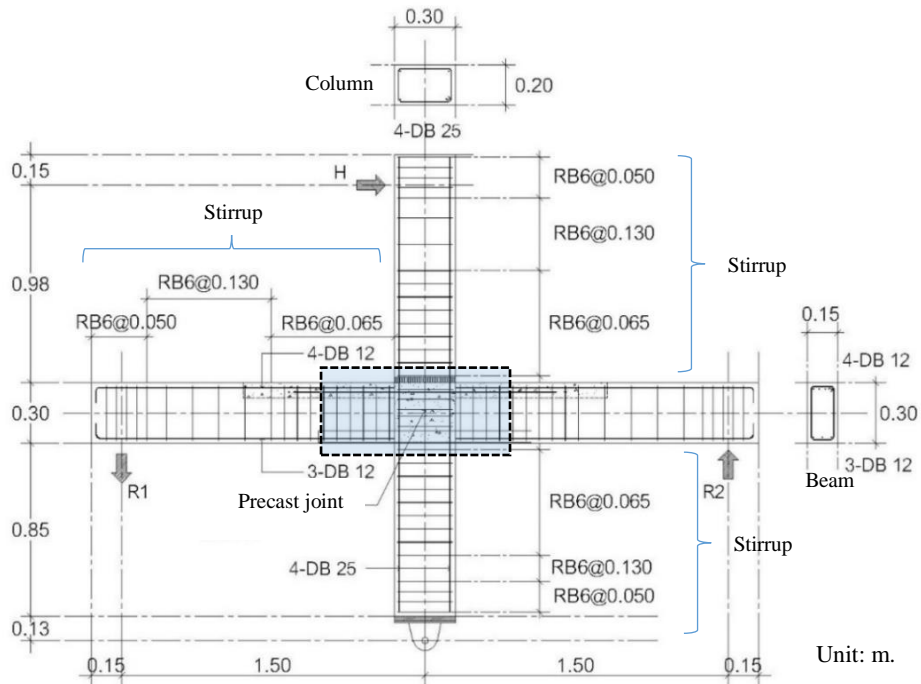

Figure 3.7 Test specimens

49

(a) Detailing of interior monolithic subassemblage frame

(b) Detailing of interior precast subassemblage frame

Figure 3.8 Detailing of test specimens

Table 3.2 Joint detail of the test specimens

Specimen	Designed parameters	Expected maximum Strength, H_{expect} (kN)	Failure Mode
M1	Monolithic	43.25	Flexural Failure
P1	T-section steel insert at middle layer + lap-splice bars at top beam	41.28/41.28	Flexural Failure/Bond Failure
P2	T-section steel insert at bottom layer + lap-splice bars at top beam	51.11/33.42	Flexural Failure/Bond Failure
P3	T-section steel insert at bottom layer + lap-splice bars at top beam + Transvers reinforcement bars	51.11/33.42	Flexural Failure/Bond Failure
P4	T-section steel insert at bottom layer + lap-splice bars at top beam + Transvers reinforcement bars + Diagonal bars	51.11/33.42	Flexural Failure/Bond Failure
P5	T-section steel inserts at top and bottom layers + with lap splice	54.06	Flexural Failure
P6	T-section steel inserts at top and bottom layers + without lap splice	54.06	Flexural Failure

3.5 Precast concrete connection installing process

The precast frame was comprised of precast beams and columns. Beam-to-beam column connections used a T-section embedded into each beam and lap-splices through the concrete joints. Steel column socket with bolted connectors was used as column-to-column connections. The precast beam generally used, was a T-section with web and flange thickness as 8 mm and 6 mm respectively. The T-section steel was 355 mm long embedded in the beam equal to 220 mm; the other part was embedded into the joint core. Moreover, 2-DB12 steel bars (500 mm long) were welded at the end of the T-section with a 50 mm weld length and a 6 mm weld leg as shown in Figure 3.9(a). The other part of the steel bars was embedded into the concrete beam. Figure 3.9(b) illustrates the interior sub-assemblage installation process with the details of specimen P2 which were only slightly different from the other specimens. Both precast beams were setup on the top edge of the bottom column. Then steel plates with a thickness of 8 mm (75 mm x 150 mm, width x length) were welded to connect both beams at the edges of the T-section

51

steel. At the top region of the beam elements, the lap-splices (1300 mm long with the same top longitudinal reinforcement amount of the beam) were used to connect between beam-to-beam and through the joints. The lap length of the spliced bars was 500 mm. The top precast column was installed by the column socket with bolted connectors. Finally, cast-in-place non-shrink grout concrete was placed into the joint core and upper part of the beams.
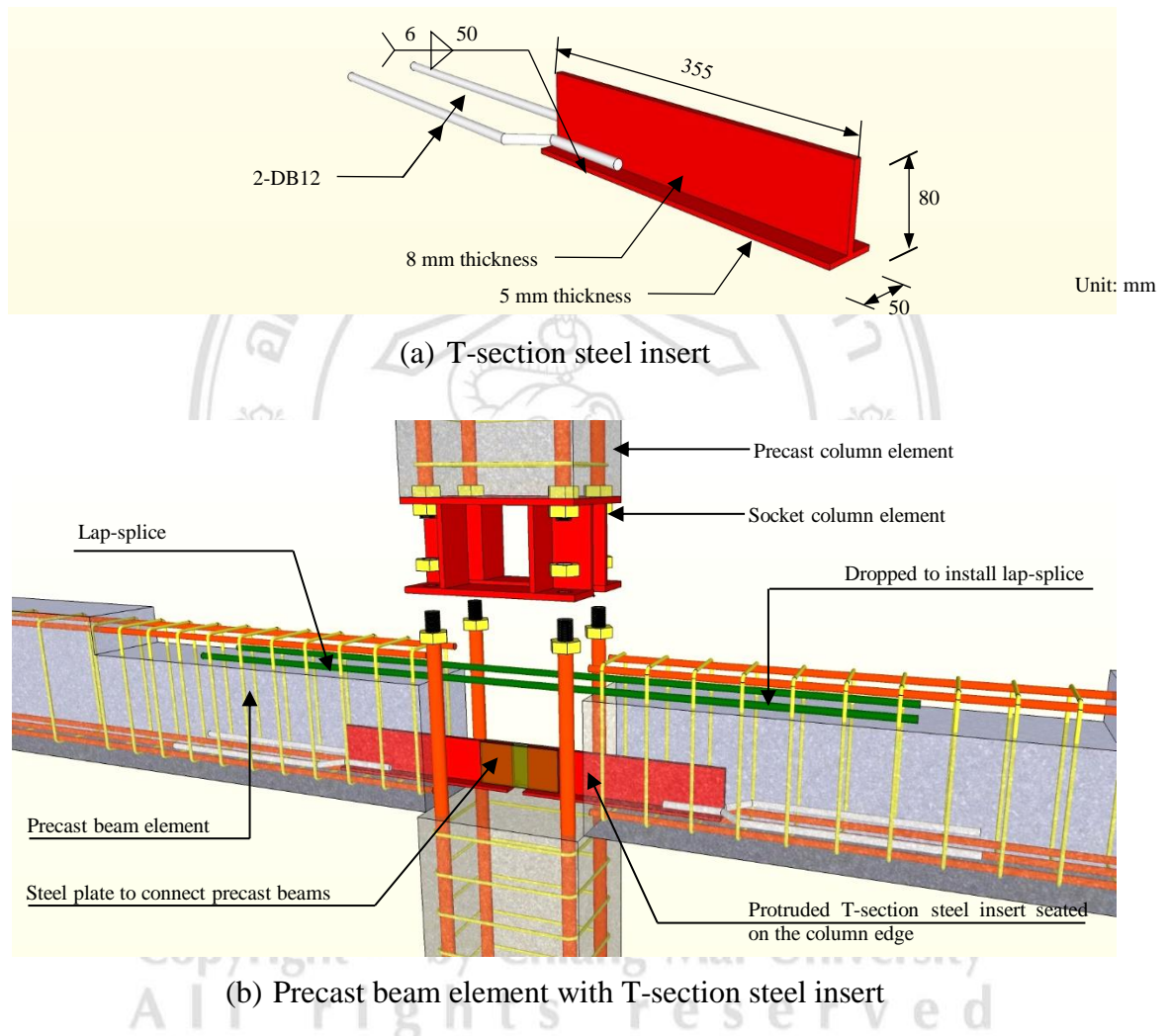

(a) T-section steel insert

(b) Precast beam element with T-section steel insert

Figure 3.9 Precast assemblage process

3.6 Connection Details

To develop the seismic performance of the precast connections, the precast connection details were compared to the monolithic connection. Furthermore, the developed precast connections, P2-P6 specimens, were against the current P1 connection. In the study, there were two kinds of the precast connection (shown in Figure 3.10) i.e. column-to-column connection and beam-to-beam connection. For the first connection,

there had been a previous study (Lertvilairut, 2012), to observe the seismic performance of the socket column connection for jointing between a precast column and RC footing. The study also proposed a new column connection for precast construction. The proposed detail of the column-to-column connection was used to assemble all precast specimens. In this study, only the beam-to-beam column precast connections were focused. The detail of the current connection, P1 connection, was redesigned and developed as P2 to P6 connections. It aimed to improve the seismic performance such as strength capacity, ductility, strength degradation and energy dissipation.
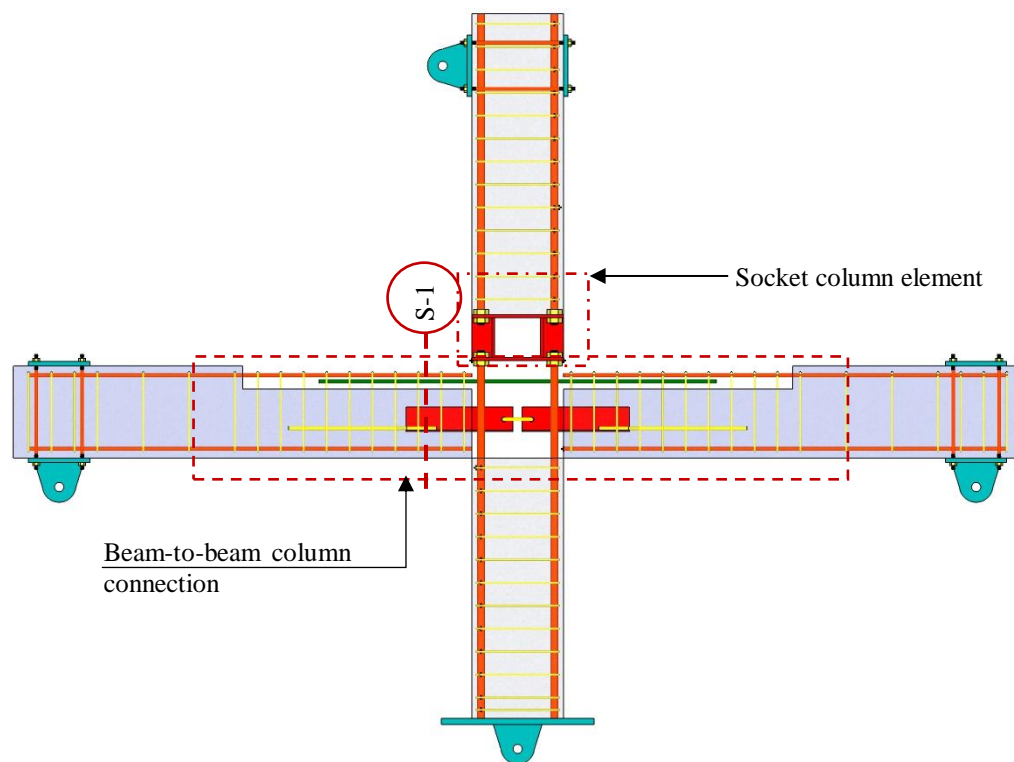

Figure 3.10 Column-to-column connection and beam-to-beam connection

The design experiment can be explained that a design assumption of the P1 precast connection for using in the current prefabricated construction was based on gravity load rather than laterally load generated during earthquake events. Furthermore, the negative bending capacities at the column face were very low because the level of T-section steels was at the intermediate region of the beam depth as shown in Figure 3.10(b). The P2 connection was modified from the P1 connection by shifting down the T-section steel to the bottom region of beam depth as shown in Figure 3.11(c), to increase the nominal bending capacities of beam section at the column face. The P3 and P4 connections and

53

beam sections were similar to P2 specimen. Furthermore, there were different details in the joint region by installing additional reinforcements, to improve the shear capacities of joint element from the P2specimen. Transverse reinforcements were installed in the beam-column joint of the P3 specimen. For the P4 specimen, both the transverse reinforcements and diagonal bars were added in the joint region. A design assumption of the P5 and P6 connection were based on relocating beam plastic hinging zones. The beam nominal moment capacity on the critical region is 1.25 times larger than the maximum anticipated moment capacity of the other beam section. Therefore, the 4-DB12 lap splices in the top beam region were replaced by using an inverse T-section steel as shown in Figure 3.11(d). The beam details of P5 and P6 specimens were very similar. However, there was a few difference in both details. It was the use of lap-splice bars at the edge of the T-section in the P5 connection but the other connection was without the lap-splices. Table 3.3 shows the summarize of connection details.
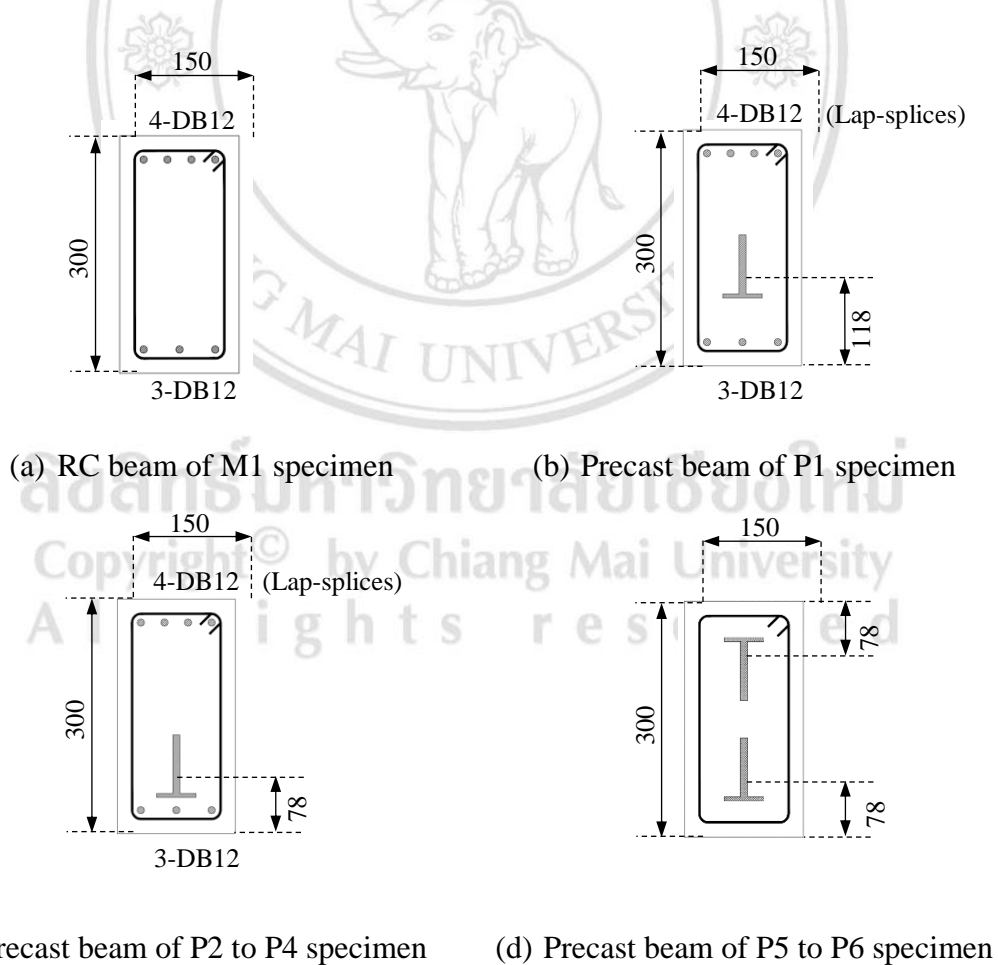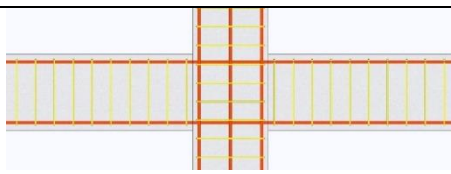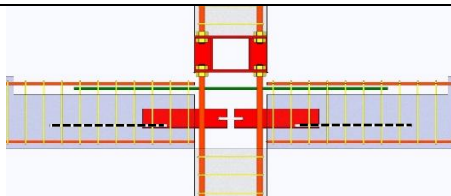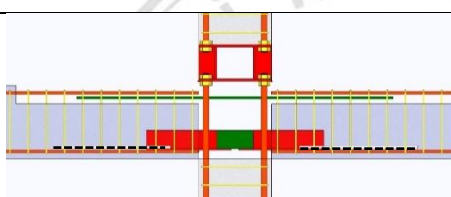

(a) RC beam of M1 specimen   (b) Precast beam of P1 specimen

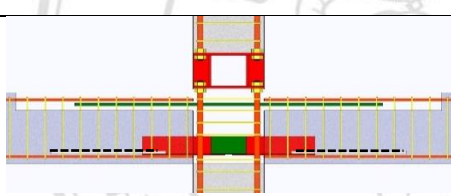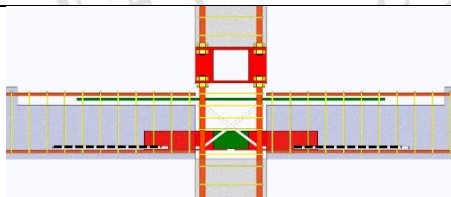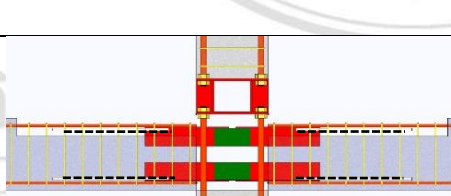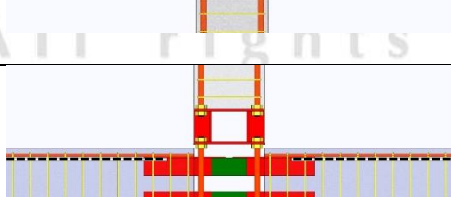(c) Precast beam of P2 to P4 specimen   (d) Precast beam of P5 to P6 specimen

Figure 3.11 Beam section at the joint region (at section S-1 in Figure 3.10)

Table 3.3 Development of joint details of the test specimens

Specimen	Joint detail	Description
M1		Reference specimen
P1		Current precast system
P2		Developed precast joint detail (shifting down the T-section steels to the bottom-depth of the beam section)
P3		Developed precast joint detail (shifting down the T-section steels to the bottom-depth of the beam section and adding the transvers reinforcement in the joint core)
P4		Developed precast joint detail (shifting down the T-section steels to the bottom-depth of the beam section and adding the transvers and diagonal reinforcement in the joint core)
P5		Developed precast joint detail with consideration of plastic beam hinging relocation (using the T-section steel inserts at top region of beam section at the column face
P6		Developed precast joint detail with consideration of plastic beam hinging relocation (using the T-section steel inserts at top region of beam section at the column face without lap-splices)

3.6.1 Monolithic specimen (M1, control specimen)

The monolithic concrete specimen was designed according to the ACI 318-14 and ACI 352R-02 (2002) for moderate-seismic regions. For the longitudinal reinforcement ratio of the beam element, the chapter 21 of ACI 318-14 allows a limit on the reinforcement ratio as 0.025. However, NEHRP: Seismic design technical brief No.1 (2008) had suggested that a beam flexural reinforcement in the joint region should be 0.01 stating that is more practical for constructability. Furthermore, a column reinforcement ratio was not excess 0.03. Therefore, the beam reinforcement ratios at the top and bottom regions were 0.0116(4-DB12) and 0.0086(3-DB12), respectively. The reinforcement ratio of the column was also 0.0118(10-DB12). For transverse reinforcement in beam and column elements, the closed stirrups were installed with spacing arrangement according to DPT 1304-54 seismic design code (2011), approximately 0.25 times of the element's depths. In the joint core, Six RB6-closed stirrups were contained in the concrete joint as shown in Figure 3.12. The test result of the monolithic specimen is used as a reference specimen, to compare the seismic performance with other precast connections in this study.
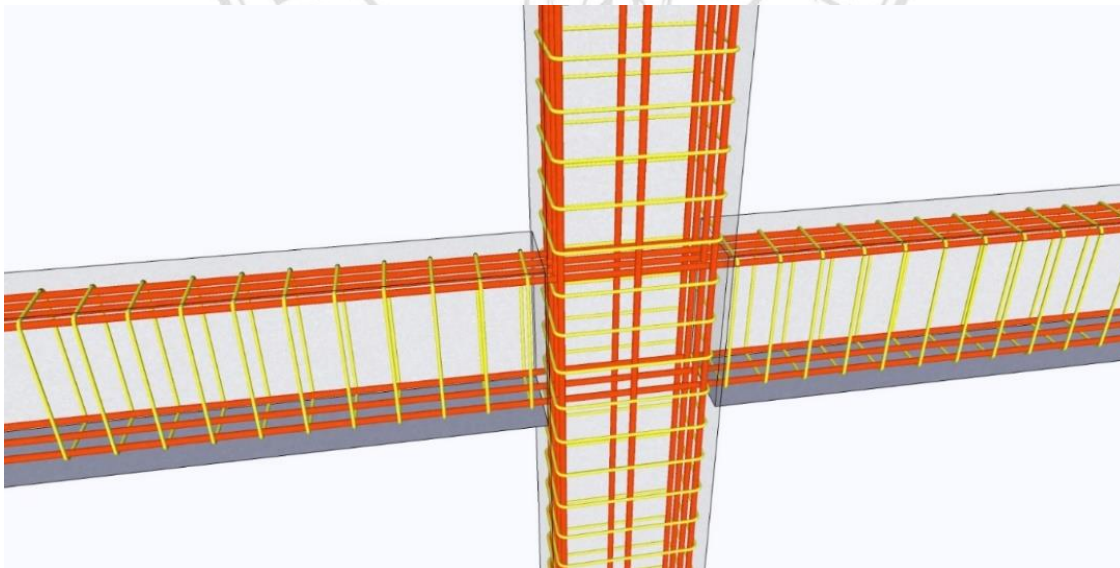

Figure 3.12 Joint detail of M1 specimen

3.6.2 Current precast connection (P1)

The P1 detail represented a precast detail for in the current prefabricated construction system at Northern Thailand region. An assumption of joint design was adopted for gravity resisting precast frame. The T–section steels were located at the middle-depth of beam section. For the connecting process, a DB-12 chain-shaped bar was input in the 15 mm diameter-holed on the T-section steels. About the top reinforcement detail, 4-DB12 lap-splices with the same steel ratio as the top reinforcement of the beam were used to connect beam-beam through the joint. There was no transverse steel in the joint as shown in Figure 3.13. For the void at joint region, high strength non-shirk grout concrete was filled.
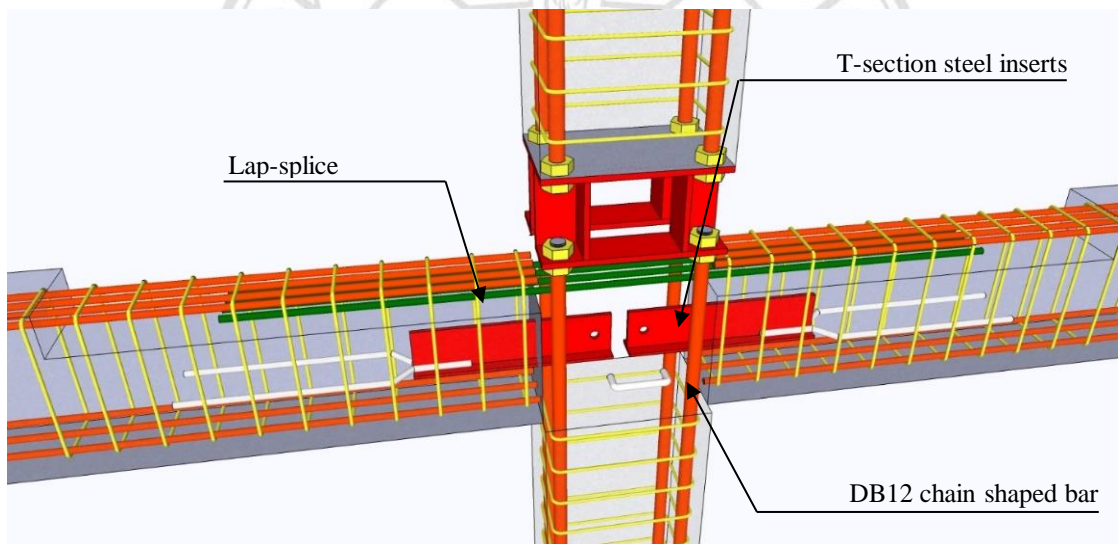

Figure 3.13 Joint detail of P1 specimen

3.6.3 Modified precast connection (P2)

Based on the P1 joint detail, the T-section steels were shifted down to the bottom-depth of the beam section, to increase a nominal flexural moment strength of the beam section at column face. To connect the concrete beams, the two steel plates were adopted by welding the steel plates with the T section steel inserts at the edges, as shown in Figure 3.14. For top reinforcement, the lap splices to connect between both beams were the same as P1 specimen.
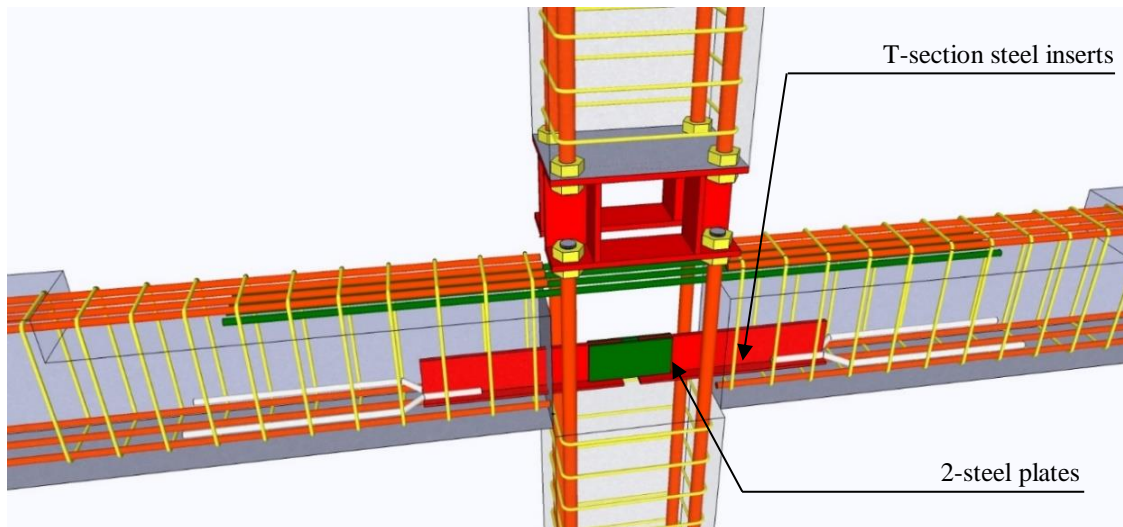
Figure 3.14 Joint detail of P2 specimen

3.6.4 Modified precast connection (P3)

The precast connection detailing within the joint of P3 specimen was very similar to those of specimen P2 excepting the inclusion of 5-RB6 stirrups in the column joint. This was to improve the confining condition of concrete in joint core, as shown in Figure 3.15.
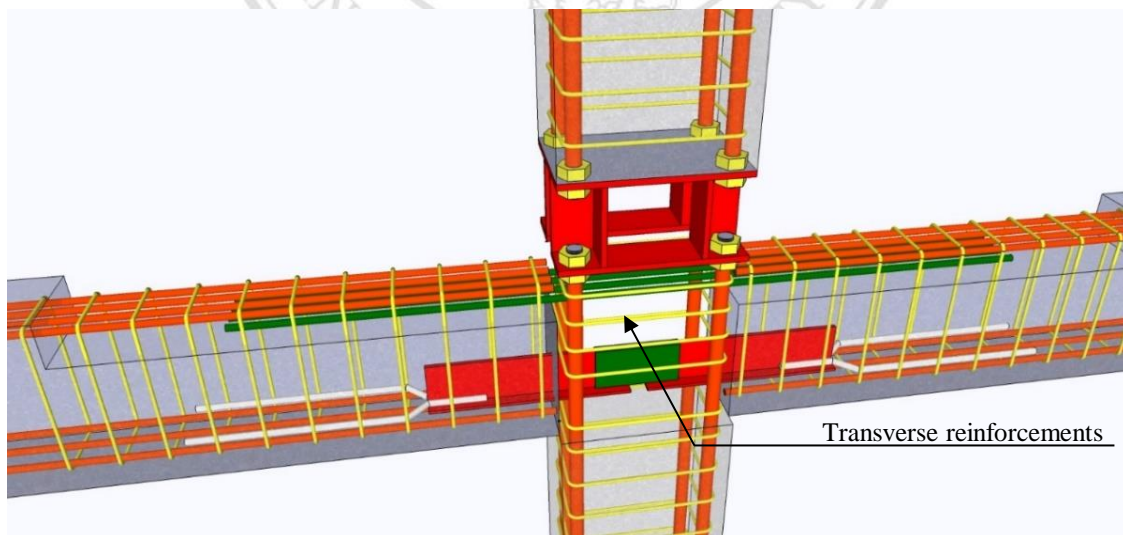

Figure 3.15 Joint detail of P3 specimen

3.6.5 Modified precast connection (P4)

The precast connection details within the joint of P4 specimen was developed from those of specimen P3. Excepting some special reinforcement, four DB12 diagonal bars were additionally installed, to improve the bond condition within joint core, as shown in Figure 3.16.
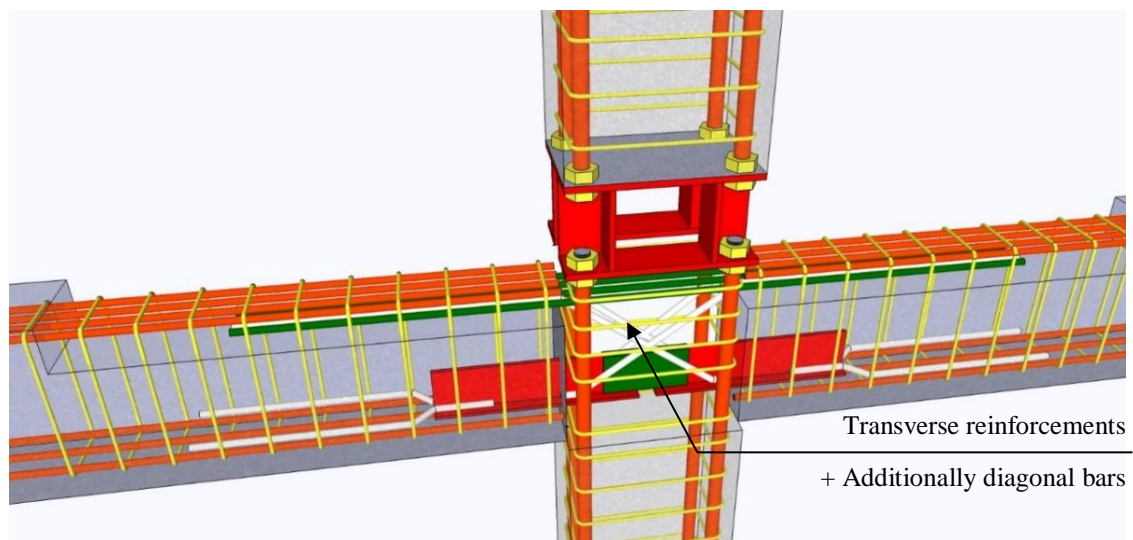

Transverse reinforcements
+ Additionally diagonal bars

Figure 3.16 Joint detail of P4 specimen

3.6.6 Modified precast connection (P5)

For the joint detail of specimen P5, the lap-splice bars, top reinforcement in joint region, were replaced by using reversed T-section steels to connect the beam across concrete joint. The joint detail was designed to relocate the plastic beam hinge by increasing the nominal flexural capacity of the beam section within one effective beam depth away from the column face which the nominal capacity is 1.25 times larger than the maximum anticipated moment capacity of the other beam section. Therefore, the beam sections at the column face were symmetrical in terms of the steel reinforcement ratio. In the installation process, four steel plates were used to connect the beam-to-beam by welding process at the edges of the T-sections both bottom and top region. The detail is shown in Figure 3.17. The aim of this detailing is to relocate the splitting crack far away from the beam ends.

Figure 3.17 Joint detail of P5 specimen
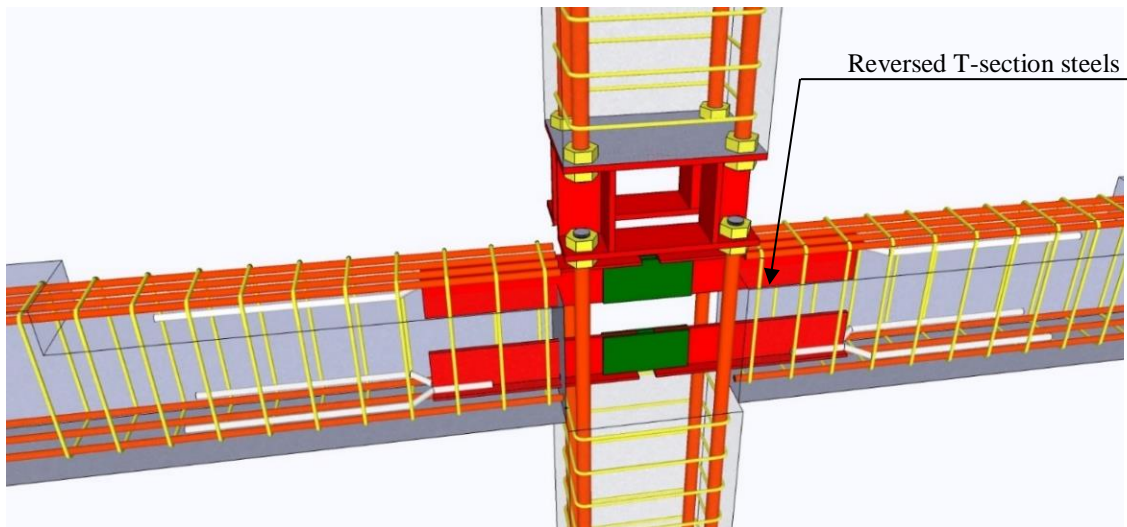
3.6.7 Modified precast connection (P6)

The joint P6 detail is developed from the P5 connection. The embedded steel bar at the edge of T-section steels in concrete beams were used to replace longitudinal reinforcement without lap splices, to improve the bond condition and prevent the splitting crake in the critical region as shown in Figure 3.18.
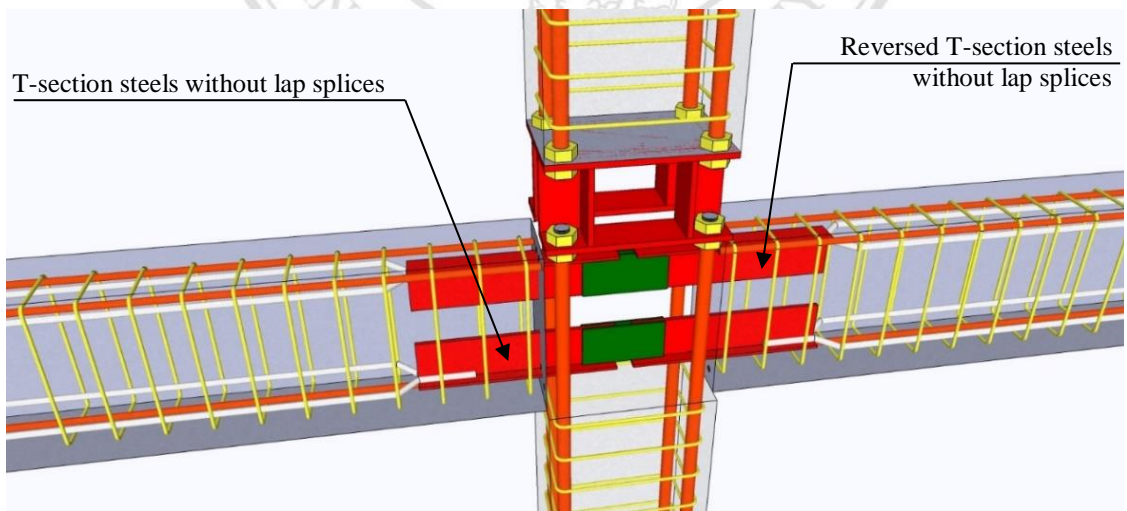

Figure 3.18 Joint detail of P6 specimen

PART B: Numerical Study

3.7 Analytical and Parametric Study

Due to the doubt of the seismic performance of the precast connections under a high column load of precast concrete frame, this chapter is aimed to analytically investigate the performance of concrete structures with the precast connections in this study. Nonlinear fiber FE modelling was adopted to predict the response of a concrete structure under reversal cyclic loading with varying column load. To achieve the necessary aim, the fiber based Finite Element Analysis using SeismoStruct V.2016 software was performed. The FEA models were first calibrated and compared with the test results. After the calibration, a parametric study was performed by varying the values of a constant column load from $0.10fc'A_g$ to $0.50fc'A_g$ to observe a P-Δ effect of the concrete structures under seismic load. The highest axial load in the parametric study was equal to $0.50fc'A_g$ because the maximum design axial load for a tied column in ACI318-14 (2014) is only permitted up to a limit of $0.80\phi P_o$ or $0.52P_o$.

3.7.1 Fiber-based finite element modeling

To simulate the test specimens in this study, the FE modelling as shown in Figure 3.19 were designated as a two-dimension problem. The FE model was composed of 20 linear beam elements and 24 nodes. Based on the fiber based finite element formulation, the cross-section was discretized into concrete and longitudinal steel fibers. A simple geometric relation between deformation of section and normal strain/fiber strain was established. Uniaxial nonlinear constitutive laws of specified materials were applied across the section area. The previous study of Yu (2006) suggested that the appropriate number of fiber should be 100-300. In this study, a typical value of the number of fibers was 200 with two integration sections. Figure 3.20 shows a comparison between the concrete beam sections (M1, P2-P4 and P5-P6 specimens) and the fiber FE beam sections at the column face. The equivalent section areas of the steel fibers were equal to the reinforcing area of the test section. The reinforcing locations of the fiber sections and the concrete section were coincided. Furthermore, there were roller support restraints applied at the beam end nodes. In addition, a hinge support restraint was attached at the bottom end node of the column. The concentrated self-weight load of the beam was considered. A constant axial force was applied on the top of the column element.
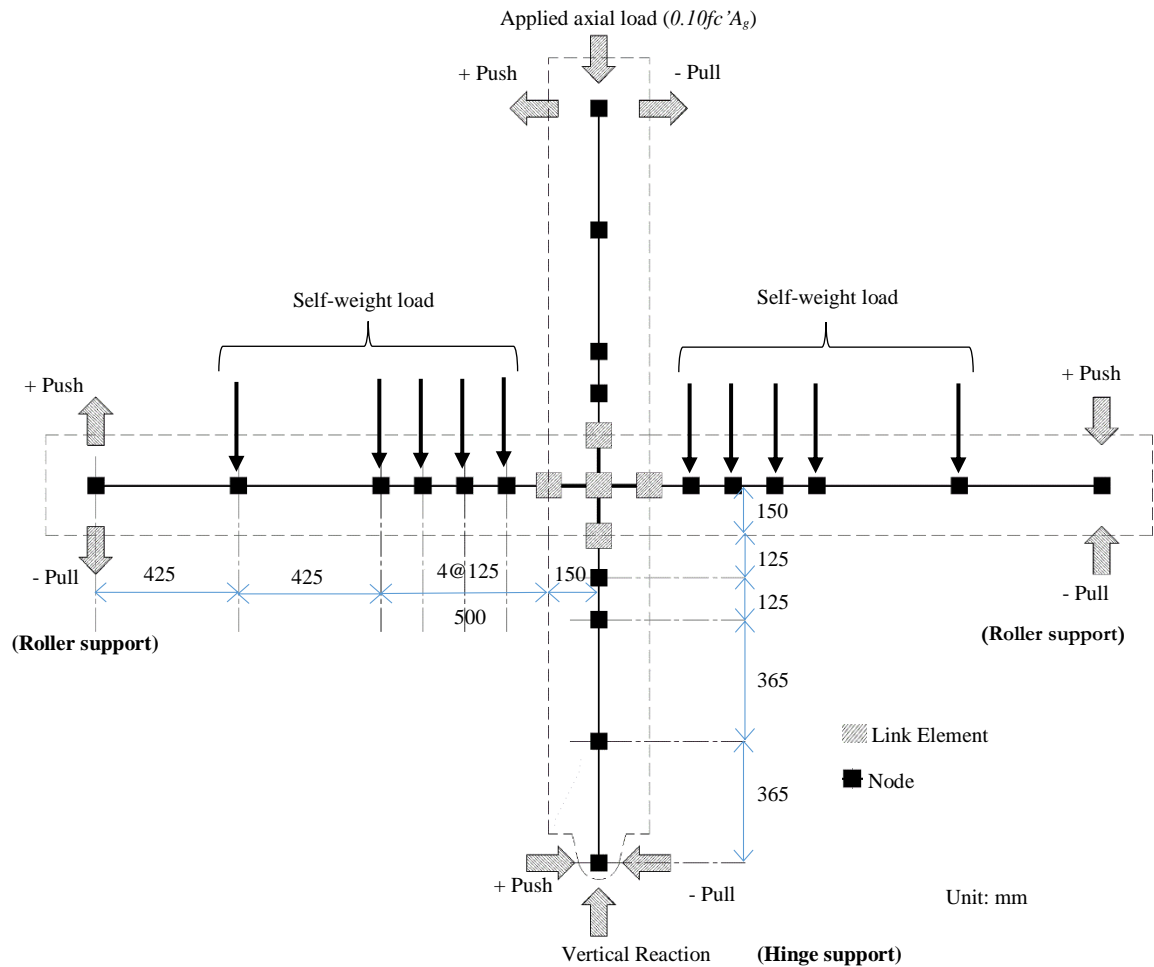
61

Figure 3.19 Fiber finite element model

For the intersection between the beam and column, the interior concrete joint was designated as the shear panel zone with 8 bar-slip springs and 4 interface shear springs. An idealization of the beam-column joint model proposed by Lowes *et al.* (2003) was adopted to simulate the complex hysteretic behavior. A constitutive model used to define these springs includes the response envelope and the unload-reload path to represent the degradation of the strength and stiffness during the reversal cyclic loading. Hence, a nonlinear response curve proposed by Takeda *et al.* (1970) was adopted to represent the force-deformation response of these springs in the beam-column joint model.

(a) RC beam of M1 specimen
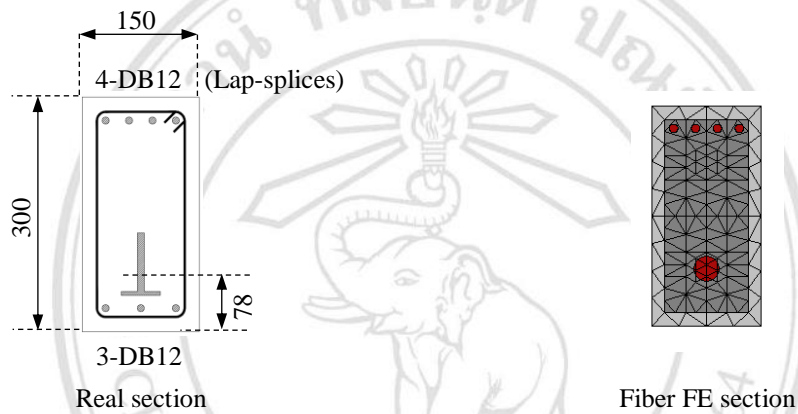
(b) Precast beam of P2-P4 specimen

(c) Precast beam of P5-P6 specimen

Figure 3.20 Comparison between concrete beam section and fiber FE section at the
column face

3.7.2 Constitutive laws

- *Concrete Model*

In this study, the Mander *et al.(1988)* concrete model as shown in Figure 3.21 was employed. Four important parameters were prepared in the concrete model as, (a) uniaxial compressive strength, $f_c = 44.03$ MPa; (b) tensile strength, f_t=4.13 MPa; (c) strain at peak stress, ε_c=0.002 and (d) the confinement factor, k_c =1.034 and 1.000 for the confined and unconfined concrete, respectively.
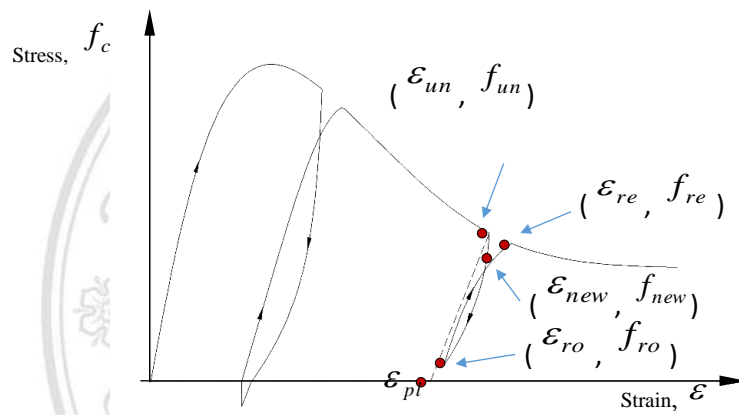
Figure 3.21 Stress-Strain relationship of concrete under cyclic loading

- *Longitudinal Reinforcement Model under Reversal Loading*

The Menegotto-Pinto model with Filippou isotropic hardening rules as shown in Figure 3.22 was utilized here. There are eight parameters composing of: (a) a modulus of elasticity of the rebar, E_s; (b) yield strength, σ_y; (c) strain hardening parameter, μ, which is the ratio between the post-yield stiffness and the initial elastic stiffness of the rebar; (d) transition curve initial shape parameter, R_0; (e) transition curve shapes calibrating coefficients, a_1 and a_2, (f) isotropic hardening calibrating coefficients, a_3 and a_4. Table 3.4 shows the eight specified parameters used in the study.

Figure 3.22 Stress-Strain relationship of Menegotto-Pinto model (1973)

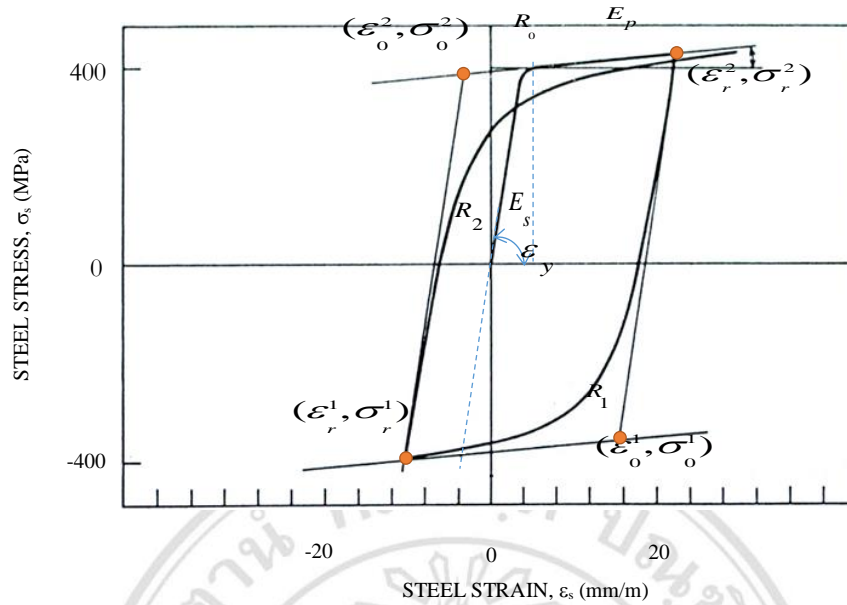Table 3.4 Specified values for parameter defining the Menegotto-Pinto steel bars model

Steel Reinforcements	E_s (MPa)	σ_y (MPa)	μ ($\frac{E_p}{E_s}$)	R_0	a_1	a_2	a_3	a_4
Longitudinal Reinforcement	215,746	454	0.0013	24.75	24.80	0.40	0.0850	7.00
Lap-splice	215,746	240	0.0067	24.11	24.00	0.20	0.0225	0.25
T-section steel	180,255	278	0.0046	24.85	24.75	0.40	0.0035	3.00

- *Beam-column joint model*

To observe the cyclic response of the concrete beam-column joints, there are three primary mechanisms to consider, i.e., (a) anchorage failure of the longitudinal bars of the beam and column members embedded in the joints, (b) shear response of the concrete joint core and (c) shear-transfer failure at the interface of the beam-joint or column-joint. Figure 3.23 shows the Lowes *et al.* joint model used in this simulation. A nonlinear spring proposed by Takeda *et al.* as shown in Figure 3.24 was applied to define the cyclic behavior of all the springs in the beam-column joint model. As shown in Tables 3.5 and 3.6, five parameters were defined in order to fully characterize this response curve, (1) yielding strength, F_y; (2) initial stiffness, K_o; (3) post yielding to initial stiffness ratio, α;

65

(4) out loop unloading stiffness degradation factor, β_o;(5) inner loop unloading stiffness degradation factor, β_1. The unloading stiffness from the post yielding point in the outer hysteresis loop can be defined as equation (3.2). The unloading stiffness in inner hysteresis loop shows in equation (3.3).

$$K_{rout} = K_o(\frac{D_y}{D_m})^{\beta_0} \qquad (3.2)$$

$$K_{rin} = \beta_1 K_o(\frac{D_y}{D_m})^{\beta_0} = \beta_1 K_{rout} \qquad (3.3)$$

Where D_y is the yielding displacement, D_m is the previous maximum displacement, K_{rout} is the unloading stiffness from the post yielding point in the outer hysteresis loop and K_{rin} is the unloading stiffness in inner hysteresis loop.
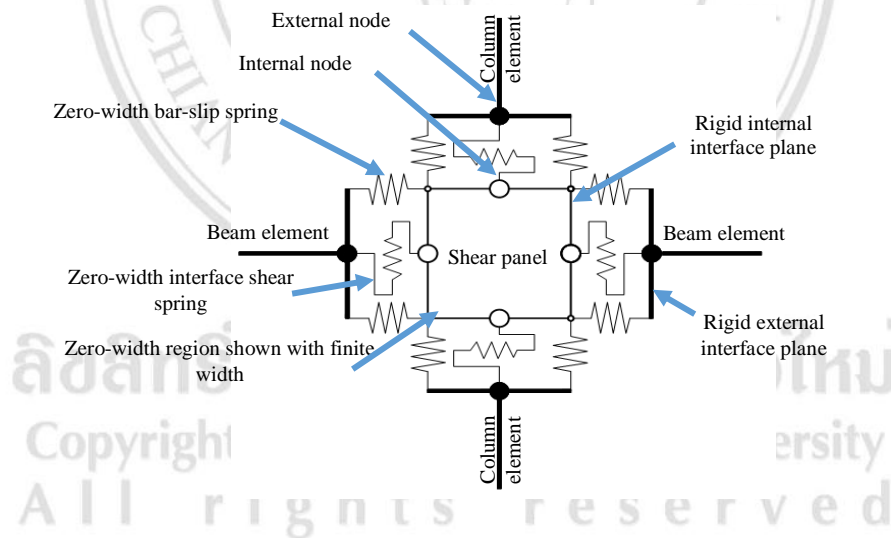

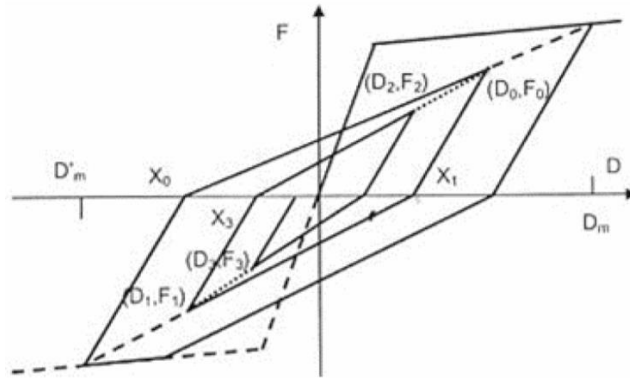Figure 3.23 Component of the beam-column joint model

Figure 3.24 The modified one-dimensional constitutive hysteresis Takeda model
(Takeda *et al.* 1970)

Table 3.5 Specified values of parameter for bar-slip rotational springs (Beam)

	F_y (kN-m)	K_o (kN-m)	α	β_0	β_1
M-FEM Series	45.48	21,130	0.035	0.10	0.225
P1-FEM Series	15.00	20,160	0.123	0.60	0.0783
P2-FEM Series	22.30	20,160	0.250	0.60	0.0783
P3-FEM Series	22.30	16,000	0.250	0.40	0.0783
P4-FEM Series	25.00	16,000	0.250	0.40	0.0783
P5-FEM Series	25.00	21,116	0.250	0.60	0.0783
P6-FEM Series	40.30	20,060	0.123	0.80	0.0783

Table 3.6 Specified values of parameter for shear springs (Beam)

	F_y (kN)	K_o (kN)	α	β_0	β_1
M-FEM Series	139.80	2,459,000	1×10^{-6}	1.0×10^{-5}	1.00
P1-FEM Series	34.98	2,459,000	1×10^{-6}	1.0×10^{-5}	1.00
P2-FEM Series	34.98	2,459,000	1×10^{-6}	1.0×10^{-5}	1.00
P3-FEM Series	34.98	2,459,000	1×10^{-6}	1.0×10^{-5}	1.00
P4-FEM Series	34.98	2,459,000	1×10^{-6}	1.0×10^{-5}	1.00
P5-FEM Series	34.98	2,459,000	1×10^{-6}	1.0×10^{-5}	1.00
P6-FEM Series	34.98	2,459,000	1×10^{-6}	1.0×10^{-5}	1.00

67

-    Lap-splice model

In the experimental study, there were lap-splices used for connecting the precast beams at the joint region. The test results in the previous chapter shows the major failure mode on slippage in the lap-splice bars at the potential beam-hinging zone, leading to the severe bond deterioration after the maximum capacities. Because the tensile splitting-cracks were developed along to the splice length. Hence, overall behavior of the structure importantly depends on the cyclic response of the lap-slices in the critical zone.
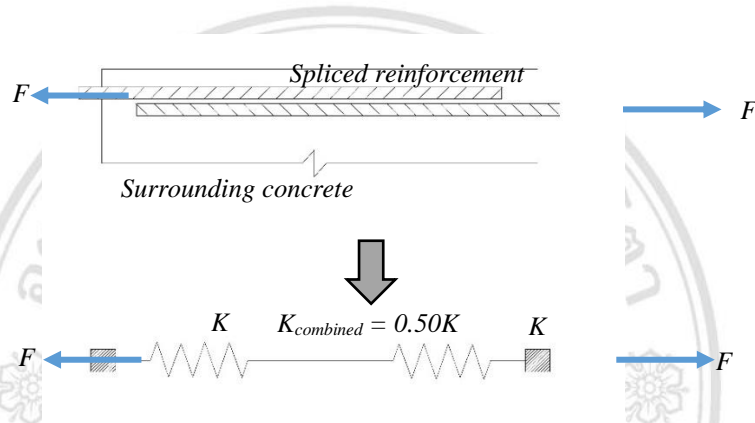

Figure 3.25 Idealization of lap-splices

F_p = Anchorage strength
F_r = Residual strength
Δ_p = Slip at failure
$\Delta_r = \Delta_p + C_o$
C_o = Clear lug-spacing of anchorage reinforcement
K_e = Elastic stiffness
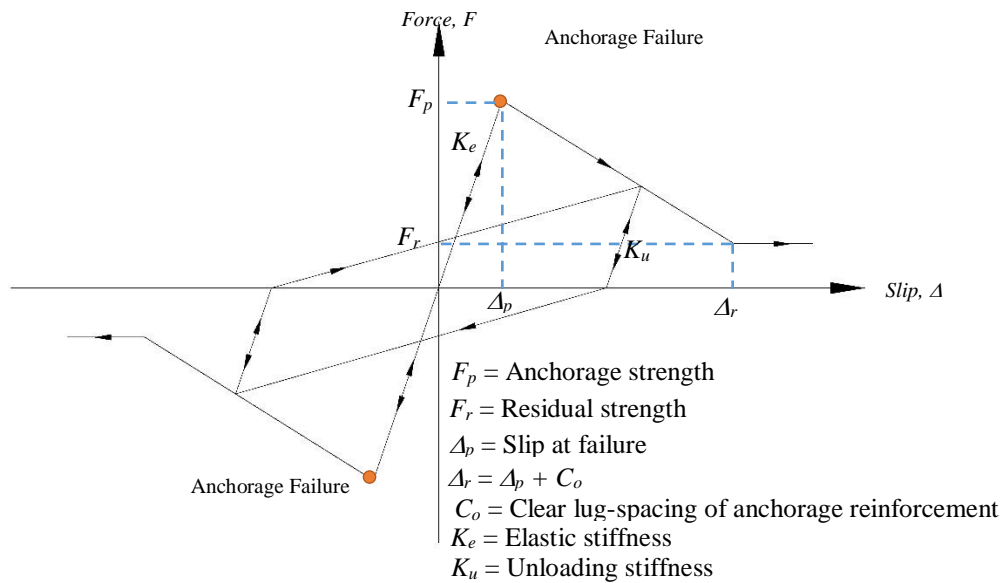K_u = Unloading stiffness

Figure 3.26 The one-dimensional constitutive hysteresis for anchorage-slip and lap-splice springs

Suthasit and Warnitchai (2008) defined the ideally lap-splice spring in the plastic hinge zone. As shown in Figure 3.25, the lap-splice reinforcement is individually

assumed to behave as an anchored reinforcement, resulting in the lap-splice spring which is modeled to 2 anchorage-slip spring. Figure 3.26 shows the backbone curve of anchorage-slip springs determined by assuming piece-wise constant bond stress distribution (Alsiwat and Saatcioglu, 1992). Furthermore, the modified-Takeda hysteresis model is performed to simulate the response the anchorage-slip springs.

3.7.3 Calibration Models

The seven FE models were performed to validate with the test results. The models could be classified according to the test specimens of one monolithic specimen and six precast specimens as shown in Table 3.7.

Table 3.7 Test specimens and finite element model in the study

Test specimen	FE model
M1 (M1-EXP)	M1-FEM
P1 (P1-EXP)	P1-FEM
P2 (P2-EXP)	P2-FEM
P3 (P3-EXP)	P3-FEM
P4 (P4-EXP)	P4-FEM
P5 (P5-EXP)	P5-FEM
P6 (P6-EXP)	P6-FEM

3.7.4 Parametric Study

It is absolutely imperative to recognize the second-order P-Δ effects when designing a building located in a seismic region. The second order effects are caused by gravity loads (P) acting on the lateral displacement (Δ), which leads to an increase of internal secondary moments in frame elements and connections. In buildings subjected to earthquake ground motion, the P-Δ effects can ultimately lead to loss of lateral resistance and dynamic instability. Some design codes such as ASCE7-10(2010) allows the negation of P-Δ effect if the calculated deflections have not exceeded the service limitations. However, ductile concrete frames have to serve large lateral displacements. In the parametric study, the applied axial force factor (α), defined in percentage of $fc'Ag$, were varied from 0.10 to 0.50 (*0.10fc'Ag to 0.50fc'Ag*), as shown in Table 3.8. This is to

69

observe the effect of the variable axial force to behavior of strength and stiffness degradation during reversal cyclic loading.

Table 3.8 Values of axial force at the top column for parametric study

Series of Parametric FE model		Factor of applied axial load(α)
M1-FEM Series	Pi*- FEM Series	
M1-FEM-P10	Pi-FEM-P10	0.10
M1-FEM-P20	Pi-FEM-P20	0.20
M1-FEM-P30	Pi-FEM-P30	0.30
M1-FEM-P40	Pi-FEM-P40	0.40
M1-FEM-P50	Pi-FEM-P50	0.50

***Pi is a name of precast specimens as P1, P2, P3, P4, P5 and P6